Active Control of Leading-Edge Dynamic Stall

David Greenblatt
Faculty of Mechanical Engineering, Technion – Israel Institute of Technology, Haifa

Abstract

The control of dynamic stall by periodic forcing was studied on a NACA 0012 airfoil under incompressible conditions by means of two-dimensional zero mass-flux blowing slots, oriented at 45° and 90° to the chord-line respectively. Time-resolved surface pressure and wake survey measurements were phase-averaged and integrated to yield the aerodynamic loads. Dynamic stall was controlled by "trapping" the bubble upstream of the forcing slot and the momentum imparted by the zero mass-flux device that was required to affect control was proportional to the square of post-stall angle of attack. Deep dynamic stall, where the static stall angle is exceeded by a large margin, was effectively eliminated but relatively large momentum coefficients, greater than 0.04, were required to achieve this. For various reduced frequencies and momentum coefficients, the 45° slot exhibited greater control authority over moment coefficient excursions than the 90° slot. A comparison of NACA 0012 and 0015 airfoils showed that for the former, stall was significantly more severe, typically requiring larger momentum coefficients to effect control, and different reduced frequency ranges were effective for the different airfoils.

Nomenclature

c	airfoil chord
C_d	drag coefficient: d/cq
C_{dp}	form-drag coefficient: d_p/cq
C_l	lift coefficient: l/cq
$\Delta C_{l,\max}$	$C_{l,\max} - C_{l,\max}$ (pre-stall)
C_m	pitching moment coeff.: m/c^2q
$C_{m,\text{exc}}$	pitching moment coefficient excursions: $C_{m,\max} - C_{m,\min}$
$C_{m,A}$	"allowable" excursions: $1.2 \times C_{m,\text{exc}}$(pre-stall)
C_p	pressure coefficient: $(p - p_\infty)/q$
C_μ	rms momentum coeff.: $\langle J\rangle/cq$
C_μ^*	minimum C_μ required to maintain $C_{m,\text{exc}} \leq C_{m,A}$
f_a	airfoil oscillation frequency
f_e	forcing frequency
F^+	reduced forcing frequency: $f_e X_{TE}/U$
h	slot height
$\langle J\rangle$	rms jet momentum: $\rho u_J^2 h$
k	reduced airfoil frequency: $\pi f_a c/U$
Ma	Mach number
p	local surface pressure
q	free-stream dynamic pressure: $\rho U^2/2$
Re	chord Reynolds number: $\rho Uc/\mu$
t	time
u_J	rms slot blowing slot velocity
$u_{J,\max}$	peak slot blowing slot velocity
U	free-stream velocity
X_{TE}	distance from slot location to trailing-edge
x/c	normalized chordwise distance
α	angle of attack
α_s	static-stall angle
μ	air dynamic viscosity
θ	slot angle relative to the chord line

ρ air density
τ dimensionless time tU/c

Subscripts
max maximum value of a coefficient
min minimum value of a coefficient

1. INTRODUCTION

Dynamic stall on rotorcraft retreating blades results in dramatic loss of lift and large pitching moments, which transmit excessive and damaging impulsive loads to the flight control system and airframe [1,2]. This so-called retreating blade stall is thus a key factor limiting maximum flight speeds, maneuverability and agility [3]. A dominant feature is the so-called dynamic stall vortex (DSV), sometimes characterized by "bubble bursting," that is generated when the blade pitches at a sufficiently high pitch rate beyond its static-stall angle [1]. Control of the DSV has historically been attempted by passive means such as leading-edge slats [4] as well as active steady blowing or suction [5]. Studies that involve passive and active flow control techniques are vital in order to meet performance projections of blade loading and maneuverability respectively [6,31].

In recent years a number of important innovations were made with regard to the control of dynamic stall, particularly under compressible conditions. This included multielement airfoil designs [8,32], dynamic leading-edge shape adaptation [33], a variable droop leading edge concept [7,34] and zero mass-flux blowing (forcing) via two-dimensional slots [9,10]. The latter method was studied under incompressible conditions on a NACA 0015 airfoil (hereafter 0015) where both leading-edge and aft forcing from a $0.75c$ slot were investigated. Due to trailing-edge stall on this airfoil, aft forcing was effective in improving airfoil performance providing that $\alpha < \alpha_s$. Leading-edge forcing enhanced flow attachment over the entire upper surface and reduced trailing-edge separation, which resulted in increased maximum lift and reduced moment excursions well into the post-stall regime. Unsteady pressure data acquired near the maximum angle of attack and phase-averaged with respect to the forcing frequency, indicated that the generation and advection of coherent structures over the airfoil surface were not significantly affected by the dynamic airfoil pitching motion [25]. An investigation conducted on a modern rotorcraft airfoil under mildly compressible conditions [10] indicated that comparable aerodynamic enhancements could be achieved in the range $0.1 \le Ma \le 0.35$, provided that the non-dimensional frequency (F^+) and momentum input (C_μ) were maintained. Thus a major challenge for attaining effective control authority at flight Mach numbers relies on actuators that can generate slot velocities at appropriate frequencies [11]. Given the difficulty associated with generating high amplitude oscillatory slot velocities, an equally important challenge involves the determination of F^+ at which the C_μ required to achieve a prescribed performance enhancement is at a minimum.

Although dynamic stall occurs near the tips of blades where compressibility effects cannot be ignored ($Ma \approx 0.4$), dynamic stall is seen to originate and persist in regions inboard, closer to the hub, where the flow can be considered to be incompressible [13]. Furthermore, although the traditional trend in aerodynamics is towards higher flight speeds *(V),* recent years have also witnessed the opposite trend, with a demand for unmanned vehicles of successively decreasing dimensions and flight speeds (so-called micro aerial vehicles – MAVs). For active flow control, this opens new opportunities with potential for substantial increases in control authority, primarily because $C_\mu \propto 1/V^2 c$. There are, therefore, several compelling reasons for studying incompressible dynamic stall control.

Studying dynamic stall control on a NACA 0012 (hereafter 0012) has merit because this airfoil is still widely used for rotor blades due to its near-ideal behavior of the center of pressure with varying angle of attack. It is also considered to be a classic "leading-edge staller." A recent investigation of incompressible static stall control on leading-edge (0012) trailing-edge (0015) stallers, noted significant differences in effective F^+ and C_μ ranges [12]. For example, larger momentum coefficients were required in the former case due to the high centrifugal acceleration experienced by the leading-edge boundary layer, and different reduced frequency ranges were found to be effective on the different airfoils. The different stalling characteristics as well as control differences manifested primarily as a result of the difference in leading-edge radius. Nevertheless, since perturbations were introduced downstream of the region of larger leading-edge curvature, and effectively trapped a leading-edge separation bubble, airfoil performance responses were proportional to C_μ. Justification for presenting data on the basis of F^+ can be found in [18] and [37].

The present study was undertaken to investigate experimentally incompressible dynamic stall on a 0012 airfoil by means of two-dimensional zero mass-flux oscillatory blowing. The specific objectives were (1) to study the basic nature of leading-edge incompressible stall and compare this with existing studies; (2) determine the conditions under which dynamic stall can be effectively controlled; (3) study the mechanism by which dynamic stall in controlled; and (4) investigate the generation of thrust combined with dynamic stall control. In specific instances, 0015 data from [9] in addition to previously unpublished data are shown to illustrate the different challenges facing leading and trailing-edge dynamic stall control.

2. EXPERIMENTAL SETUP & TECHNIQUES

The 0012 airfoil model was constructed from aluminum (203 mm chord; 610 mm span), instrumented with 50 surface pressure ports and incorporated two, two-dimensional leading-edge slots (see fig. 1a for leading slot locations and coordinate definitions). The leading-edge slots were located at 5% chord (upper surface slot in fig. 1a) and 4% chord (lower surface slot in fig. 1a) and orientated at $\theta = 45°$ and $90°$ to the chord-line respectively. These corresponded to angles of 32° and 73° relative to the upper and lower airfoil surfaces respectively. Their location and orientation were dictated primarily by practical considerations. Roughness strips (Grit #100), used to trip the boundary layer, were fixed to the leading-edge and extended to 4% chord on both upper and lower surfaces. The airfoil was also equipped with a slot at 73% chord oriented at 45° to the chord line, but zero mass-flux blowing from this slot produced insignificant changes to the static aerodynamic coefficients [12] and thus it was not studied presently. The 0015 airfoil differed from the 0012 mainly with respect to the leading-edge slot, which produced a wall-tangential jet at the leading-edge (see fig. 1b). See [9] and [12] for more details of the 0015 experimental setup.

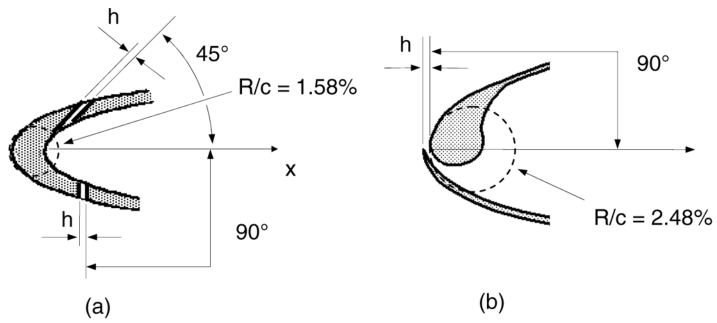

Figure 1. Leading-edge slot detail of the (a) NACA 0012 airfoil; and (b) NACA 0015 airfoil.

In order to capture representative pressure distributions, the pressure ports spacings were based on the results of a potential flow and boundary layer solver in the range $0° \le \alpha \le 20°$. The airfoil was supported internally by aluminum ribbing that rendered an effectively hollow interior, which served as a plenum chamber. All slot widths measured 0.6 mm; they were sealed for baseline (no control) measurements and when forcing was applied the slots that was not in use was sealed. For the data presented in this paper, slots were employed independently (never simultaneously) and calibrated by hot-wire anemometry. The energy content of forcing frequencies employed was at least one order of magnitude larger than the second harmonic and hence the slot calibration was based on peak velocity measurements thus: $C_\mu = (h/c)(u_{J,\max}/U)^2$. Calibrations were performed periodically throughout the experiments a total of 10 times and the amplitude uncertainty remained $\Delta C_\mu / C_\mu \le 20\%$. Lift, form-drag and pitching moment were computed by integrating the surface airfoil pressures. Airfoil drag or thrust was quantified by means of a wake survey that comprised a traversable rake of total head probes mounted at $x/c = 5$. Surface and wake pressure ports were connected to a PS4000® multi-channel array of pressure transducers (AA Lab Systems) via flexible tubing. Pressure signal attenuation and phase-lag in the tubing was accounted for by means of direct calibration and corrections were applied by using an FFT/inverse-FFT approach that is fully described in [23]. Surface pressure and wake data were augmented by hot wire measurements in the upper surface boundary layer and surface mounted tufts were used for rudimentary flow visualization.

Using the model described in [23] for pressure measurement correction, the diameter of the present 0012 pressure ports was increased by a factor of 2, the Scanivalve® pressure scanner was eliminated and each pressure port was connected directly to its own, independently calibrated, piezo-resistive pressure transducer and the pressure tubes were significantly shortened. The combination of all three of these modifications had a dramatic positive effect on the attenuation and phase-lag of the pressure signal. With the cumulative effect of all of these factors taken into account, using more than three harmonics in the correction showed no meaningful difference in the corrected pressure signal.

The airfoils were mounted in a low-speed, low-turbulence, closed-loop wind-tunnel where dynamic pitching about the airfoil $^1/_4$ chord was achieved using the pitch drive system of [27]. The Plexiglas® tunnel windows were connected directly to, and pitched with the airfoil models thereby preventing three-dimensional tip leakage effects. A shaft-mounted encoder signal was used to ascertain the instantaneous angle of attack, where errors associated with the encoder translated to angle of attack uncertainty of less than 0.1°. Zero mass-flux blowing was achieved using the device of Bachar [28]. The device consists of a circuit incorporating a blower, a siren-type flow "chopper" and a vent. The flow is driven in the circuit by the blower while the chopper produces oscillatory flow in the circuit. Air is sucked in and blown out of the circuit, through the vent, in an oscillatory manner and hence the net output of air from the vent is zero. The device was mounted outside of the wind tunnel and the vent was connected to the airfoil plenums via a flanged, flexible pipe. More details regarding the design of the device can be found in Seifert *et al* [41]. Most of the test were conducted for $0.4 \leq F^+ \leq 4$ and $C_\mu \leq O(1\%)$ with pitch oscillations at $0.05 \leq k \leq 0.15$ for $240{,}000 \leq Re \leq 480{,}000$. The control of deep dynamic stall and combined dynamic stall control and thrust generation were studied at $Re = 100{,}000$. The data acquisition rate was adjusted, depending upon the airfoil pitch rate, to acquire 180 points per cycle and aerodynamic coefficients were based on the phase-averages of at least 25 airfoil oscillation cycles. Because no phase relationship was enforced between the airfoil oscillation and the forcing frequency, 25 cycles were typically sufficient to eliminate the high frequency signature from the pressure data.

Uncertainties were estimated at: $\Delta C_l = \pm 0.01$; $\Delta C_d = \pm 0.001$; and $\Delta C_m = \pm 0.002$; respectively. No pitching-blowing phase relationship was enforced due to the large disparity between the respective frequencies: $f_e >> f_a$. Further details of the setup, including unsteady pressure measurements on the static airfoil, can be found in [12].

3. DISCUSSION OF RESULTS

3.1. Objectives of Control

The definition of *dynamic stall control* is prone to some subjectivity and thus the present data is assessed on the basis of two different metrics (see below). In order to define the various quantities of interest consider the 0012 static and dynamic data shown in figs. 2a to 2c, where the pitch-up and pitch-down motions are indicated by solid and hatched lines respectively. Dynamic data is shown for pre-stall [$\alpha = 6° + 5°\sin(2\pi f_a t)$; $\alpha_{\max} = \alpha_s$] and post-stall [$\alpha = 9° + 5°\sin(2\pi f_a t)$; $\alpha_{\max} > \alpha_s$] cases (here $\alpha_s = 11°$ and $k = 0.05$). Pre-stall pitch oscillations produce loops in the aerodynamic coefficient data: counterclockwise for C_l and C_m and clockwise for C_{dp}. On the upstroke the lift curve is below the 2π

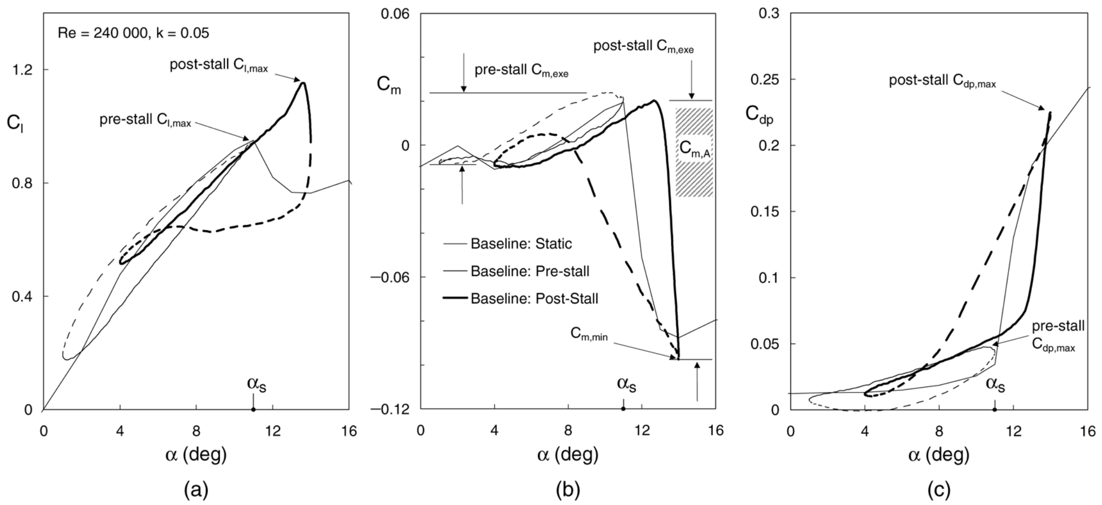

Figure 2. Illustration of objectives and definitions used for quantifying dynamic stall control; NACA 0012 data.

line and on the downstroke it is above. This behavior is predicted by purely theoretical considerations, i.e. by modifying the boundary conditions in the continuity equation, including the unsteady term in Bernoulli's equation and accounting for the unsteady wake. This is discussed in detail in [24]. The distortion of the loops observed presently bears a strong similarity to 0012 data acquired at higher Reynolds numbers [24]. From these pre-stall data we note $C_{l,\max}$(pre-stall) which is virtually identical to the static value. For purposes of comparing baseline and control data we furthermore define pitching moment coefficient excursions: $C_{m,\text{exc}}$(pre-stall) = $C_{m,\max} - C_{m,\min}$ and time-mean form and total drag coefficients: $\bar{C}_{dp}$ and $\bar{C}_d$.

In the post-stall case, when $\alpha_{\max} > \alpha_s$, the dynamically pitching airfoil continues to generate lift as is well known. This leads to moment stall, typified here by large negative pitching moment or moment excursions ($C_{m,\min}$ or $C_{m,\text{exc}}$) followed lift stall. An analysis of dynamic stall data on a wide variety of airfoils showed that for each a unique relationship exists between maximum lift, minimum moment and maximum form drag [13]. These were expressed as the "dynamic stall functions": $C_{l,\max}=f(C_{m,\min})$ and $C_{l,\max} = f(C_{dp,\max})$ and were used to evaluate dynamic stall control techniques. This metric is useful because it immediately indicates the merit of a control method. For example, an increase in $C_{l,\max}$ is only of merit if $C_{m,\min}$ does not decrease or $C_{dp,\max}$ does not increase. A different metric has been proposed that requires increasing or maintaining $C_{l,\max}$ while containing C_m to be commensurate with the pre-stall excursions, or so-called "allowable" excursions: $C_{m,A}$ [9]. A value of $C_{m,A} = 1.2 \times C_{m,\text{exc}}$(pre-stall) was suggested and will be employed here, but clearly the degree of control is subjective, because it is ultimately dictated by practical considerations such as allowable design loads, etc. In the discussions below, use is made of both of these metrics.

3.2. Leading-Edge vs. Trailing-Edge Dynamic Stall

Dynamic aerodynamic coefficients' dependence on α (figs. 3a-3d) and pressure coefficient distributions at $\alpha_{\max}$ (figs. 4a and 4b) are shown for both airfoils ($\alpha_{\max} = \alpha_s+3°$ and $\alpha_{\max} = \alpha_s + 4°$ for the 0012 and 0015, respectively). These data serve two purposes: they illustrate the difference between baseline (uncontrolled) dynamic stall on the two airfoils; and they show the different consequences of effective control (discussed in the next section). As noted above, the dynamically pitching 0012 generates lift beyond α_s without a significant change in the lift slope ($dC_l/d\alpha$). At $\alpha > \alpha_s$ (here α_s + 1.6°), $dC_l/d\alpha$ increases and this coincides with the onset of moment stall (cf. [1]) which is abrupt and relatively severe (resulting in large $C_{m,\text{exe}}$). In contrast, the dynamically pitching 0015 does not significantly increase lift beyond α_s and $dC_l/d\alpha$ decreases, with C_l remaining approximately constant up to α_s + 2°. This is accompanied by relatively gentle moment stall with relatively small excursions.

These differences were scrutinized further by considering the upper-surface C_p distributions at incrementally increasing angles beyond α_s and the main points are summarized here. At α_s + 1°, the 0012 pressure distribution showed no sign of impending boundary layer separation, but at α_s + 2°, corresponding to early stages of moment stall, reduced pressure was evident at $0.05 \le x/c \le 0.4$, consistent with a bubble bursting mechanism as discussed below [14,31]. With further increases in angle of attack, $C_{l,\max}$ was attained and the separated region propagated further downstream, reaching the trailing-edge at approximately α_s + 3°. The simultaneous sharp increase in leading-edge pressure (see fig. 4a) resulted from the reduction in curvature of the streamlines near the leading-edge that is associated with the separated flow and is reflected by the drop in C_l. As the airfoil continued to pitch-up to $\alpha_{\max,}$ complete separation engulfed the upper surface.

Two widely accepted explanations of incompressile dynamic stall have been proposed. The first is based on the so-called Van Dommelen-Shen [15] interaction, where fluid particles are driven upstream by the adverse pressure gradient and collide with slower-moving particles "ahead" of them closer to the leading edge. This results in the movement of fluid particles away from the surface, resulting in the break-away and ultimate rollup of the DSV. The second mechanism is described as an extension of the bubble bursting mechanism, presuming that a bubble already exists in the leading-edge region at $\alpha < \alpha_s$ (e.g. [14]). This mechanism may, however, be superseded by shock-induced dynamic stall for compressible flows ($Ma > 0.3$) [14,35].

The bubble bursting mechanism is believed to be responsible for dynamic stall observed here, much like that for the case of an airfoil that is pitched quasi-statically into the post-stall regime. To illustrate this, the upper surface instantaneous C_P in the leading-edge ($x/c < 0.05$) and aft-region ($x/c > 0.4$) are shown on the static airfoil that is set at $\alpha = \alpha_s + 1°$ (see figs. 5a and 5b). The time-mean C_P at incipient stall ($\alpha = \alpha_s$) is also plotted for comparative purposes in both figures. At $\alpha = \alpha_s$, the pressure is nearly

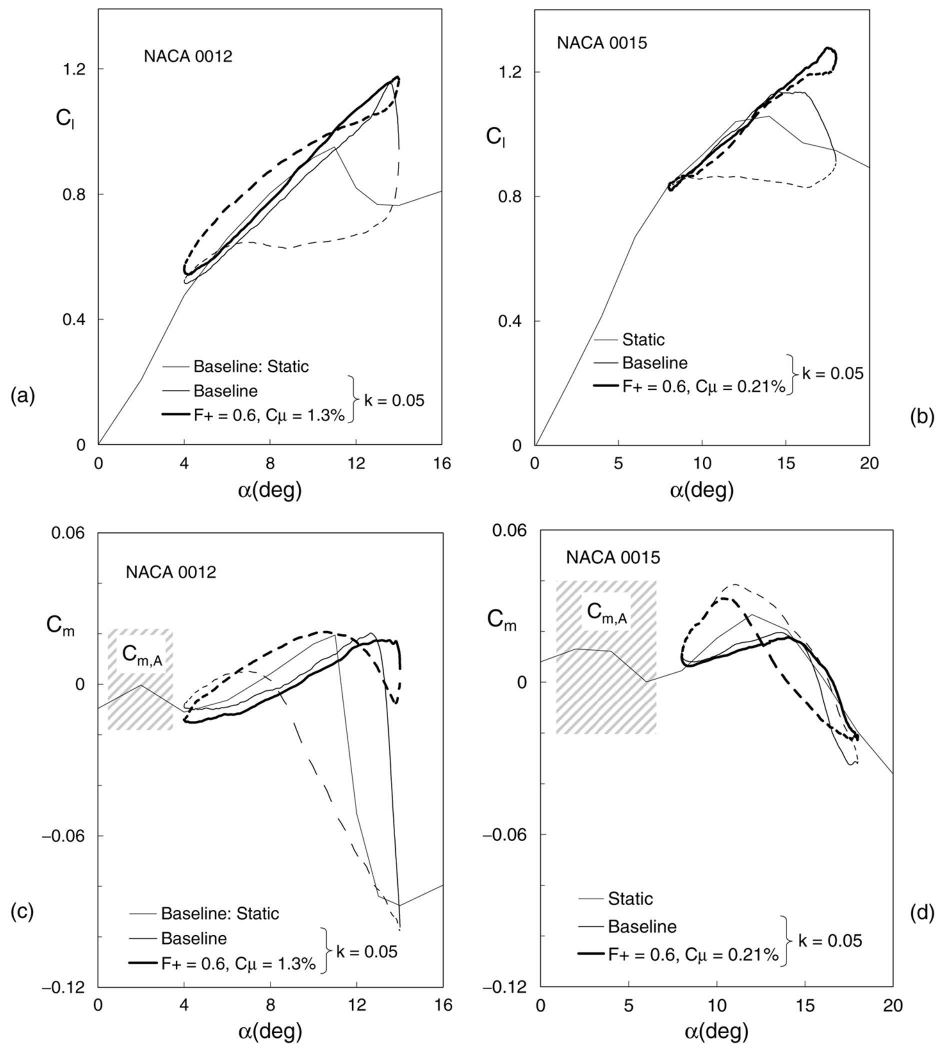

Figure 3. Comparison of NACA 0012 (45° slot; *Re* = 240,000) and 0015 (*Re* = 300,000) dynamic stall control at $F^+ = 0.6$.

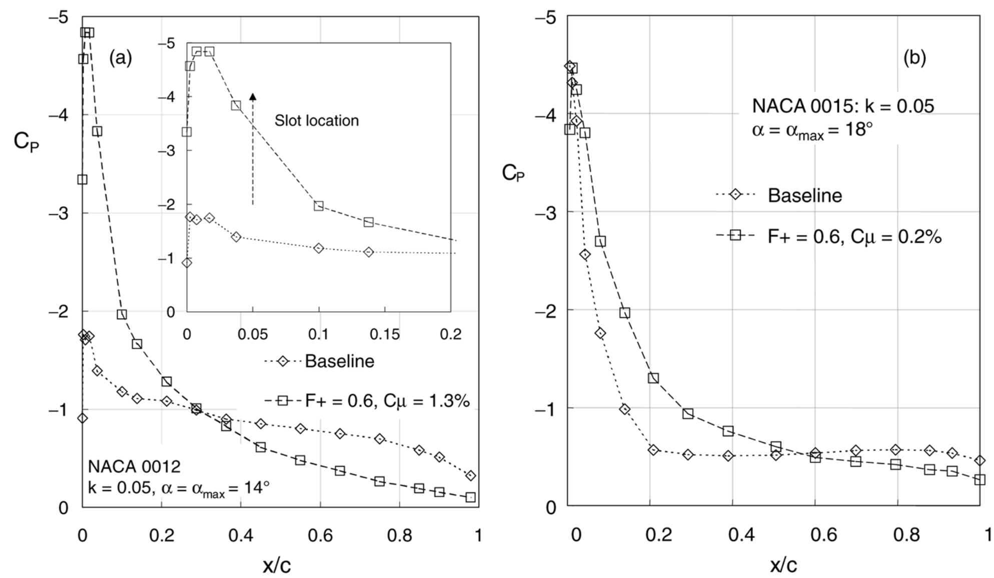

Figure 4. Comparison of upper surface NACA 0012 and 0015 pressures at maximum angle of attack.

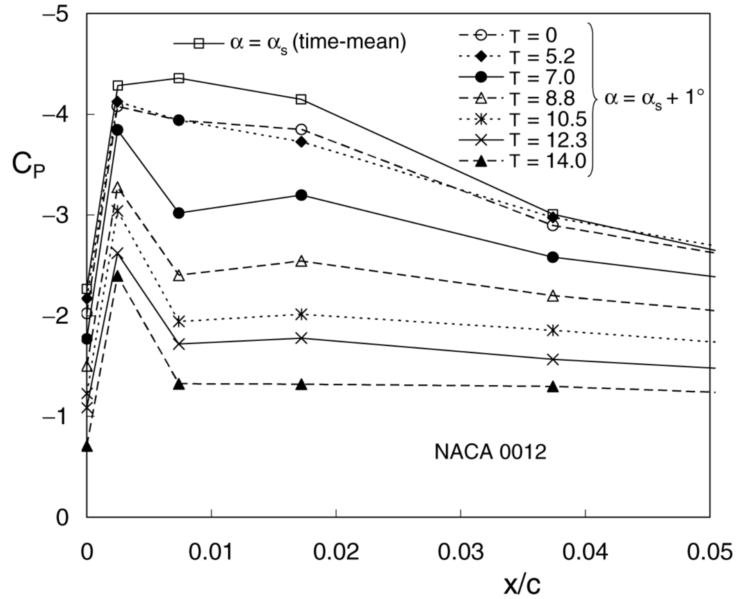

Figure 5a. Unsteady leading edge upper surface pressure coefficients on the static NACA 0012 airfoil.

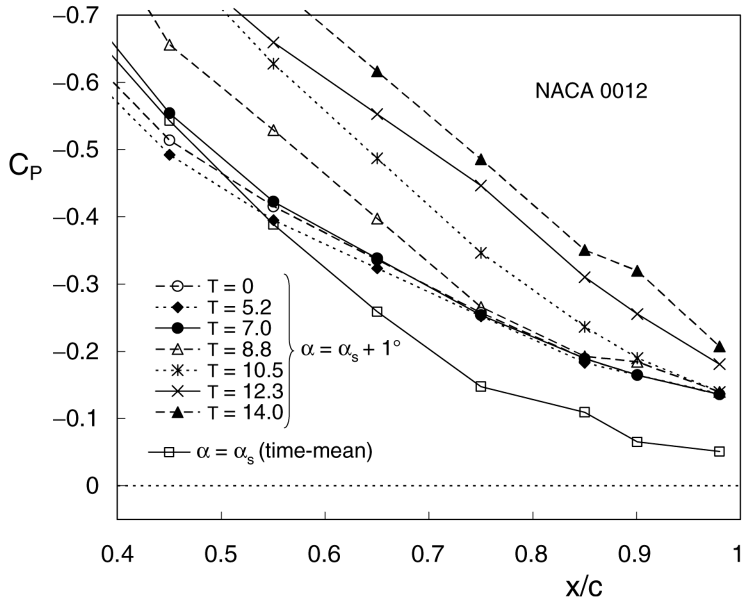

Figure 5b. Unsteady aft upper surface pressure coefficients on the static NACA 0012 airfoil.

constant near the leading-edge, followed by a steep pressure recovery and this indicates the existence of a separation bubble extending up to $x/c \approx 0.03$ (fig. 5a) (see [39] and [40]). Hence, it can be concluded that the roughness strip forces transition in the separated shear layer which then reattaches, forming the bubble. These observations are fully consistent with both high and low Reynolds number observations on the 0012 airfoil [14,35]. Examination of the trailing-edge region (fig. 5b) shows that incipient separation is evident at $\alpha = \alpha_s$ and surface-mounted tufts confirmed these observations.

With an increase in angle of attack to $\alpha = \alpha_s + 1°$, the flow began to separate and partially reattach in a quasi-periodic manner [9]. The two-dimensionality of this process was confirmed using upper surface tufts and essentially represented dynamic separation and reattachment on a stationary airfoil. Data are plotted for a typical unsteady separation event from $\tau = 0$ to 14. Examination of the leading-edge pressures clearly shows that the leading-edge bubble "bursts", as evident by the sharp pressure increase in the leading-edge region at $\tau = 7.0$ (fig. 5a). Further aft on the airfoil ($x/c > 0.4$), at the same instant, the pressures are unaffected (fig. 5b; note the different C_P and x/c scales). With increasing time, the leading-edge pressures increase rapidly, and the separated region is seen to progress further downstream (fig. 5b), reaching the trailing-edge at $\tau \approx 10.5$. The bubble-bursting mechanism is presumed to be initiated by the high centrifugal acceleration of the flow as it negotiates the leading-edge radius [11]. Potential flow calculations (using a vortex panel method) show that the peak local acceleration (U^2_e/R) at α_s is twice as large on the 0012 as it is on the 0015. It is not clear, however, what triggers the quasi-periodic partial-attachment and separation observed presently. Unlike the 0015, the 0012 leading-edge radius plays a crucial role in determining the nature of stall. Thus, the introduction of a 0012 slot at $x/c = 0$, similar to that of the 0015, would have altered its leading-edge radius and possibly its stalling characteristics.

McCroskey et al [30] observed similar partial-attachment and separation on a 0012 airfoil pitching in a quasi-steady manner beyond the static-stall angle at typical rotorcraft Reynolds numbers (see [22]). Furthermore, Currier & Fung [14] analyzed the data of McCroskey et al [30] and determined that bubble bursting was the mechanism responsible for stall. They further ascertained that in sub-critical (incompressible) cases the bubble-bursting mechanism is also responsible for dynamic stall, i.e. when the airfoil is dynamically pitched beyond the static stall angle at rotorcraft reduced frequencies.

Consideration of the pressure coefficients associated with the dynamically pitching airfoil indicated that the unsteady stalling mechanism was the same for both the static and the dynamically pitching airfoils, consistent with the observations of [14]. The main difference is that, when the airfoil is pitched dynamically, the bubble bursts under a larger streamwise pressure gradient which results in faster propagation of the separated region over the upper surface. It was also observed that the rate of bubble bursting is strongly dependent on the dimensionless pitch-rate k.

In contrast, the 0015 stalls gently from the trailing-edge and the separated flow propagates upstream with increasing α, reaching $x/c \approx 0.2$ at $\alpha_{\max}$ (fig. 4b). Thus, there is no leading-edge bubble-bursting phenomenon and no appreciable dynamic stall vortex at these relatively low angles. The substantially different dynamic stalling mechanisms have important consequences for control, as will be described below.

3.3. Dynamic Stall Control

Leading-edge control of dynamic stall is also shown in the data of figs. 3 and 4. To remain consistent with [9], "allowable" moment coefficient excursions were maintained at 20% larger than pre-stall [$C_{m,A} < 1.2 \times C_{m,\text{exc}}$(pre-stall)], which are 0.04 and 0.06 for the 0012 and 0015 respectively (see hatched sections in figs. 3c and 3d). The larger 0015 excursions arise as a result of the pre-stall aerodynamic center moving ahead of the ¼ chord location. This has been observed previously [16,17] and is apparently due to the relatively large trailing-edge included angle. Previous experience with the 0015 under both static [18] and dynamic conditions [9] indicated that relatively low reduced frequencies ($F^+ < 1$) were capable of exerting control at relatively modest forcing amplitudes ($0.1\% \le C_\mu \le 0.5\%$). The example illustrated in figs. 3b and 3d, with forcing at $F^+ = 0.6$ and $C_\mu = 0.21$, shows a simultaneous increase in $C_{l,\max}$ with a virtual elimination of hysteresis and a reduction in $C_{m,\text{exc}} < C_{m,A}$. For the 0012, with forcing from the 45° slot at the same F^+, substantially larger C_μ was required to achieve $C_{m,\text{exc}} < C_{m,\text{A}}$ although moment stall was not totally eliminated. Moreover, larger C_μ did not significantly affect $C_{l,\max}$ due to the mainly attached flow in the post-stall regime. Note, however, that the post-stall 0012 and 0015 moment excursions were reduced by factors of 4 and 1.3 respectively.

Pressure distributions (figs. 4a and 4b) show important differences in the nature of control. For the 0015, control qualitatively improves the pressure recovery, although the flow remains partially separated as can be seen by the low trailing edge C_p. In contrast, control appears to "trap" the leading-edge bubble upstream of the forcing slot on the 0012 (see inset in fig. 4a) where this mechanism is identical to that associated with static control [12]. The pressure recovery downstream indicates mild flow separation near the trailing-edge, where this is responsible for the gently moment stall seen in fig. 3c.

A summary of $\Delta C_{l,\max}$ data for a variety of F^+ as a function of C_μ is presented for both airfoils (figs. 6a and 6b); in the latter case only the two most effective reduced frequencies ($F^+ = 0.6$ and 1.1) are presented. Recall that the 0012 generates a larger baseline $\Delta C_{l,\max}$ than the 0015 due to reduced trailing-edge separation as the airfoil pitches beyond α_s and also due to the low pressure associated with bubble bursting. Therefore, for the range of C_μ considered here (<2%), forcing at a variety of F^+ does not materially affect $C_{l,\max}$; in some instances it is even slightly reduced due to the elimination of the low pressure associated with bubble bursting. Even though baseline $\Delta C_{l,\max}$ is lower on the 0015, forcing has a significant impact, with $\Delta C_{l,\max} > 0.3$ at high C_μ. Note, however, that this effect is not proportional to C_μ as has been observed before with regard to static and dynamic stall control.

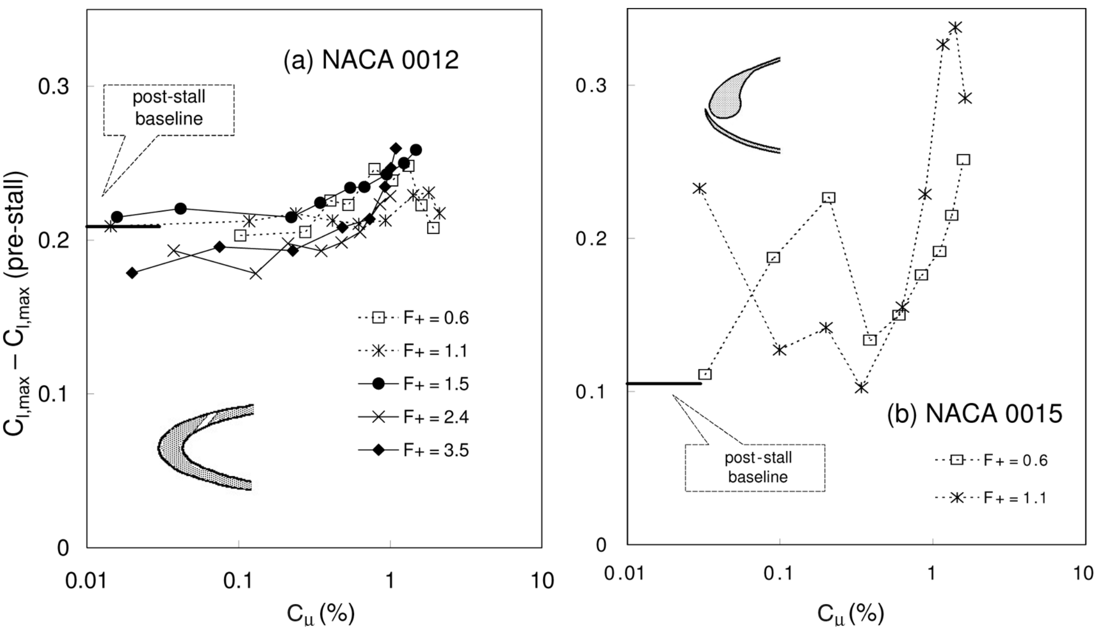

Figure 6. Overall comparison of NACA 0012 (45° slot) and 0015 lift variation at various F^+ and C_μ.

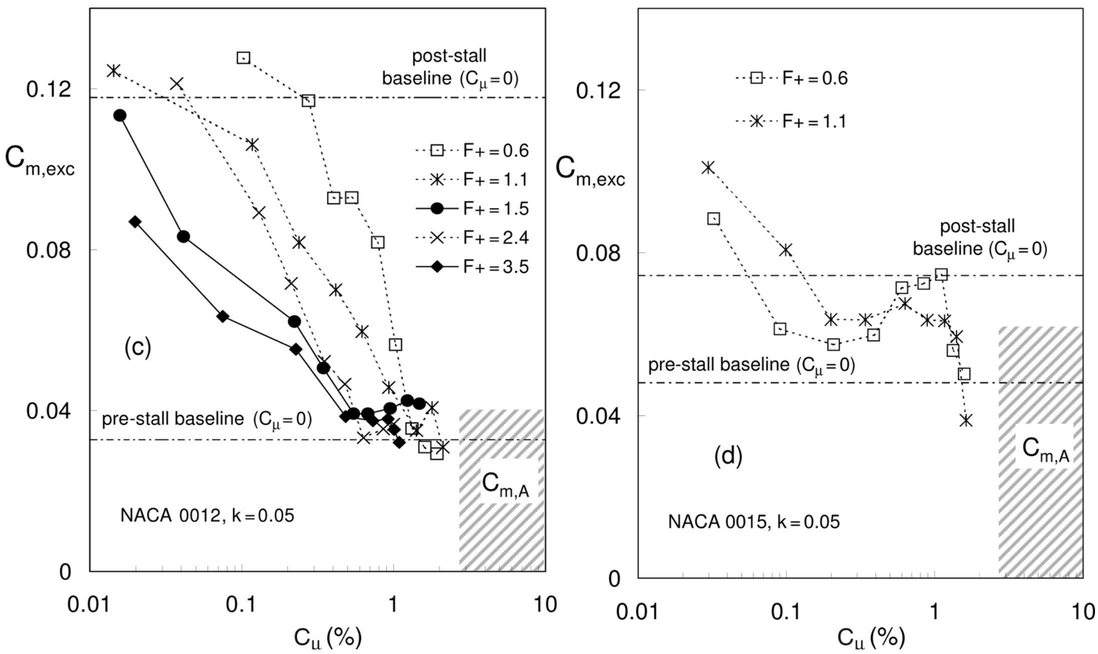

Figure 6. (contd.) Overall comparison of NACA 0012 (45° slot) and 0015 moment coefficient excursions at various F^+ and C_μ.

Corresponding $C_{m,\text{exc}}$ data for the 0012 (see figs. 6c) show a strong sensitivity to F^+ that is different in nature and substance to that of the 0015 (fig. 6d). On the 0012, an increase in C_μ produces a direct decrease in $C_{m,\text{exc}}$ irrespective of F^+, such as when C_μ exceeds some threshold, it is seen that $C_{m,\text{exe}} \propto \ln(l/C_\mu)$. In fact, $F^+ = 0.6$ and 1.1, that were observed to be the most effective for 0015 control (i.e. requiring the lowest C_μ), are the *least effective* for 0012 control – this is consistent with static data [12]. This retrospectively explains the relatively large C_μ required for effective control at $F^+ = 0.6$ shown in figs. 3a and 3c. Presently, the most effective reduced frequency is $F^+ = 3.5$ and requires approximately 4 times less C_μ than at $F^+ = 0.6$ to render $C_{m,\text{exc}} < C_{m,A}$ and up to 30 times less C_μ in order bring about a meaningful reductions in the moment coefficient excursions $C_{m,\text{exc}}$. As observed previously [9], the degree to which forcing reduces $C_{m,\text{exc}}$ on the 0015 varies in a non-proportional manner that is dependent on F^+ (fig. 6d).

In traditional active separation control, an increase in C_μ is generally associated with an improvement in performance prior to complete reattachment. The atypical behavior displayed by the 0015 is unfavorable from a practical control point of view but is intriguing none-the-less. An inspection of the slot geometry (inset in fig. 6b) and location shows that forcing takes the form of a wall-jet over a relatively highly curved surface, with $\delta/R = O(10\%)$. Flows of this nature are centrifugally unstable [19] and therefore centrifugal (Görtler) instabilities might coexist, and compete, with inflectional (or Kelvin-Helmholz) instabilities generally associated with separation control. This impact of Goertler vortices formed by a wall jet over a convex surface was clearly shown by [36] even in fully turbulent flows. Similar observations have been made [20] where separation control was studied in transitional flows with strong streamwise curvature.

The time-mean drag coefficients acting on the 0012 are presented in fig. 7 for data corresponding to $F^+ = 1.5$ and 3.5. For pre-stall excursions, the form drag is approximately 75% of the profile drag, where the remaining 25% is presumed to be due to skin friction $(\overline{C}_{df})$. For the post-stall baseline case, the form drag contribution dominates with $\overline{C}_d \approx \overline{C}_{dp}$. Consistent with the data presented in fig. 6c, increases

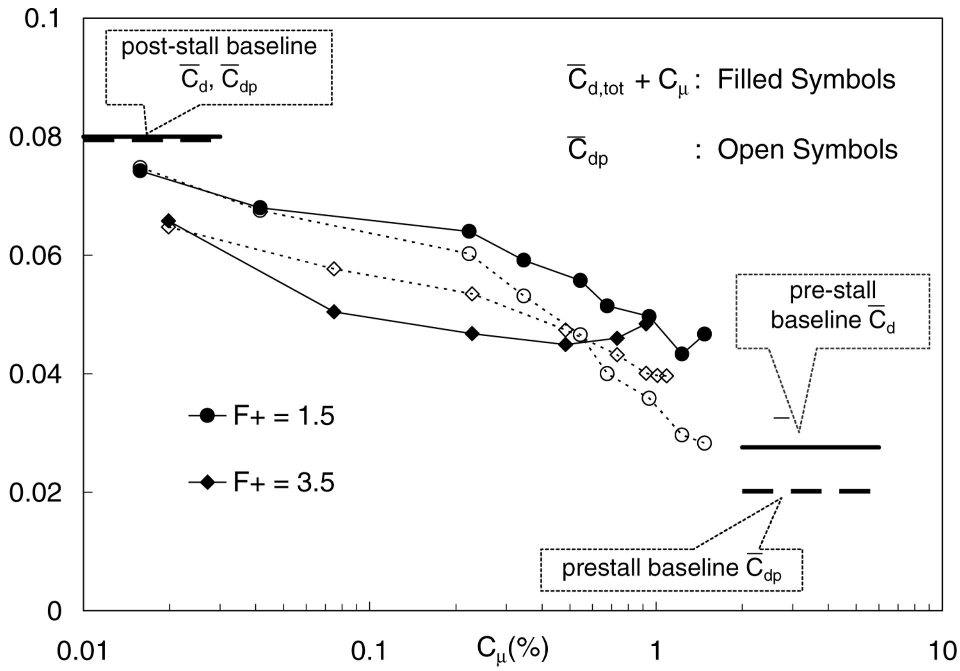

Figure 7. Comparison of form drag and total drag coefficients for the NACA 0012 (45° slot) at various F^+ and C_μ. The ordinate is indicated by the symbols type.

in C_μ bring about substantial reduction in mean drag although the total drag measured by the wake survey is the profile drag minus the thrust produced by the blowing slot. This statement can be rearranged to produce an expression for the mean skin friction coefficient based on measured quantities, namely:

$$\overline{C}_{df} = [\overline{C}_{d,\mathrm{tot}} + C_\mu] - \overline{C}_{dp} \tag{1}$$

where the first and second terms on the right hand side of equation (1) terms are plotted in fig. 7 for increasing C_μ at two reduced frequencies. For $F^+ = 1.5$, at relatively low momentum coefficients, the two terms are similar indicating that the contribution of $\overline{C}_{df}$ is small, but further increases in C_μ indicate that the flow attachment increases. At $F^+ = 3.5$, in the forcing range $0.08\% \le C_\mu \le 0.5\%$, the result is reversed with the second term larger than the first. The maximum difference (−73 drag counts) is comparable to the skin friction coefficient on one side of a flat plate at $Re = 240{,}000$. This "negative drag" remains valid even when accounting for the total uncertainty associated with equation (1), which can be expressed as ±24 drag counts. It therefore appears that, on average, reverse flow exists on the airfoil surface and thus produces skin friction thrust; careful velocity profile measurements in precisely controlled flows [29] appear to qualitatively support this observation. Note that in equation (1) above, it is assumed that all of the control C_μ is recovered as thrust; if this is not the case then the skin friction thrust would be larger.

As a result of zero mass-flux blowing, the reaction drag force produced on the airfoil is $C_\mu \cos(\theta - \alpha)$ and the reaction lift force is $C_\mu \sin(\theta - \alpha)$. In considering $C_\mu \leq 0.5\%$, this produces a lift reaction force $C_l \approx 0.003$. In this analysis we have assumed that all of the zero mass-flux momentum is recovered as thrust, i.e. $\cos(\theta - \alpha) \approx 1$. Taking the slot angle into account will lower the $\overline{C}_{d,\mathrm{tot}} + C_\mu$ even more. Therefore, this assumption is conservative and does not materially change the above conclusions.

3.4. Effect of Slot Orientation

A preliminary comparison of 0012 slot orientation under static conditions [12] showed that the 45º slot exerted larger control over $C_{m,}$ while the 90º slot produced slightly higher $C_{l,\max}$. Presently, a comparison between the two slots is made under dynamic conditions $\alpha = 9° + 5°\sin(2\pi f_a t)$, $k = 0.05$, with $C_\mu < 1.5\%$, where control from both slots effectively control moment stall (see figs. 8a and 8b). Note, however, that three-times more C_μ is required by the 90º slot in order to eliminate moment stall.

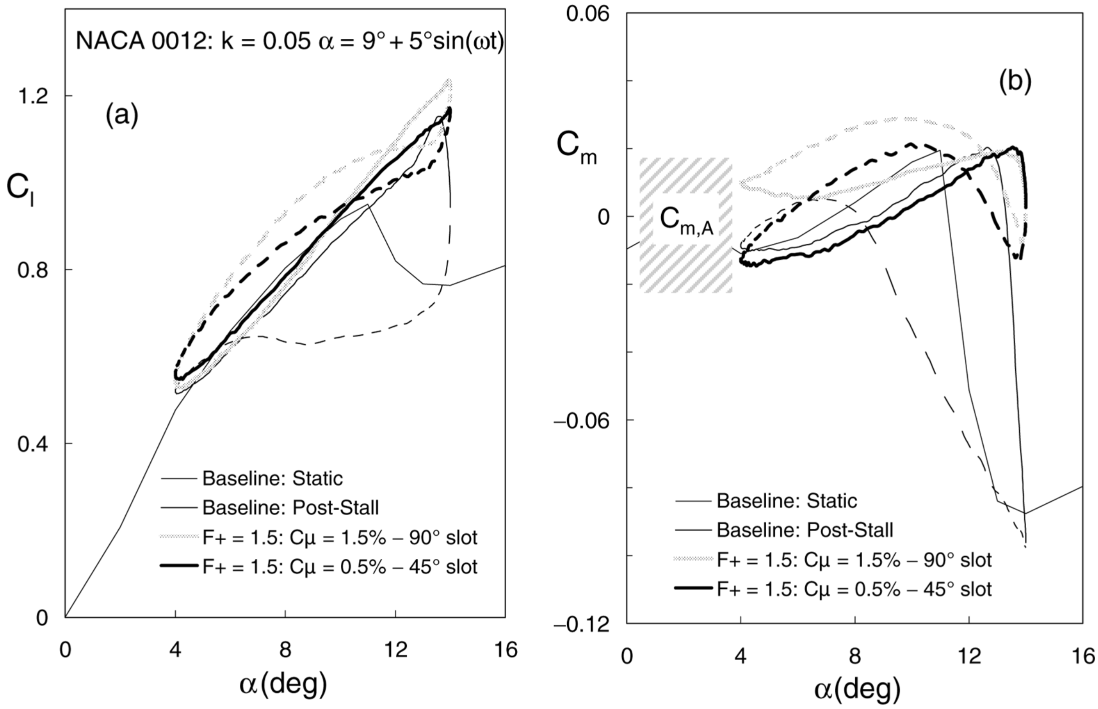

Figure 8. Effect of slot orientation on NACA 0012 dynamic stall control at $F^+ = 1.5$

The higher C_μ also results in slightly enhanced $C_{l,\max}$.

The slots were further compared for the two most effective forcing frequencies, namely $F^+ = 1.5$ and 3.5 (see fig. 9a and 9b). Neither of the two slots produced significant variations in $\Delta C_{l,\max}$ although the 45º slot at $F^+ = 3.5$ was the only case where lift was consistently enhanced for all C_μ considered. All cases showed an approximately linear variation of $\Delta C_{l,\max}$ with C_μ, where $dC_{l,\max}/dC_\mu$ was largest for the 90° slot at $F^+ = 1.5$ (curves are least-squares linear; note the abscissa log-scale). Regarding $C_{m,\mathrm{exe}}$ control, the 45° slot was consistently superior to the 90º slot and there was less sensitivity to F^+ associated with the latter. The differences in C_μ required to achieve an arbitrary reduction in $C_{m,\mathrm{exe}}$ varied between a factor of three to an order of magnitude. However, with sufficient C_μ, the 90° slot was also capable of reducing $C_{m,\mathrm{exe}}$ to typical pre-stall values.

In summary, the 45° slot is superior to the 90° slot since the former is far more effective with regard to $C_{m,\mathrm{exe}}$ reduction, while neither substantially affected lift.

3.5. Control of Deep Stall & Thrust

A common, yet demanding, test case is deep dynamic stall control where the airfoil pitches well beyond

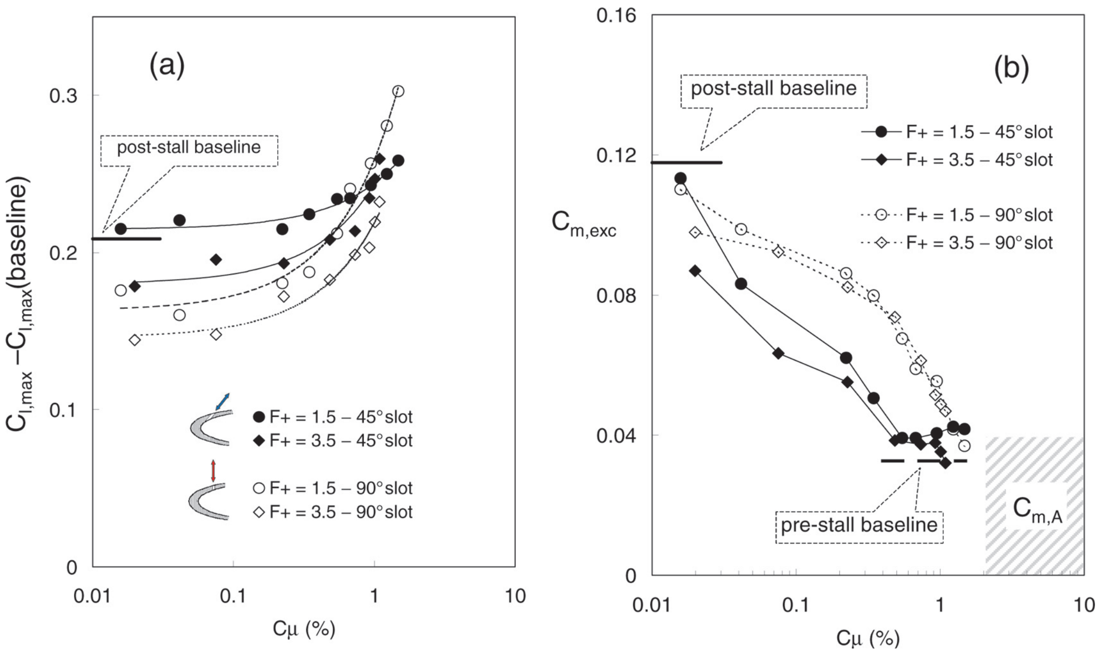

Figure 9. Effect of slot orientation on NACA 0012 dynamic stall control at various F^+ and C_μ.

the static stall angle resulting in massive separation from the upper surface that is commensurate with the chord dimensions [21]. The difficulty associated with controlling "deep stall" is appreciated when it is realized that no control methods have been successful that are consistent with the criteria and metrics described in section 3.1. Presently, control of such a scenario was attempted under the conditions: $\alpha = 10° + 10°\sin(2\pi f_a t)$ [i.e. $\alpha_{max} - \alpha_s = 9°$], at $k = 0.05$ and 0.1. It was observed under static airfoil conditions [12] that high-amplitude, high frequency actuation ($F^+ > 3$) was completely ineffective under deep stall conditions. In addition, for $Re = 240{,}000$, the actuator was only capable of producing $C_\mu < 2\%$ and this was not sufficient to fully control moment stall. This necessitated reducing the Reynolds number to that typical of MAVs, i.e. $Re = 100{,}000$, that facilitated a corresponding increase in C_μ (see e.g. figs. 10-13). For these cases the baseline dynamic $C_{l,max}$ is approximately twice the static value and both lift and moment stall are particularly severe.

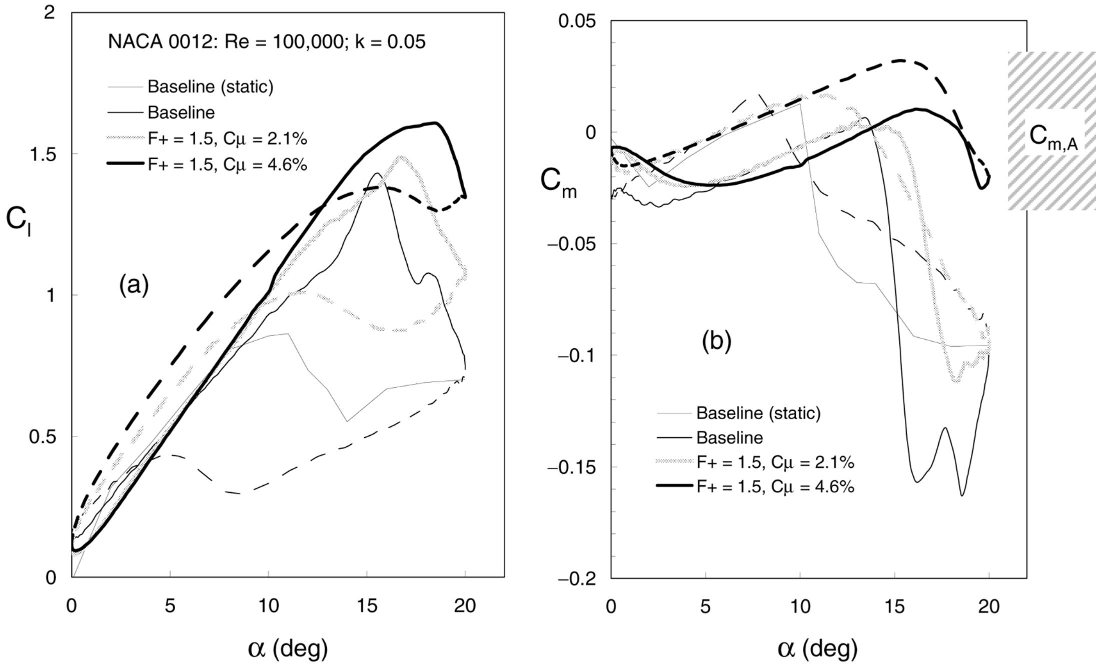

Figure 10. NACA 0012 deep dynamic stall control (45° slot) at intermediate excitation amplitudes: $k = 0.05$.

Figs. 10a and 10b further demonstrate the large amplitude required to produce effective 0012 control; note that the physical forcing frequency was reduced in order to maintain $F^+ = 1.5$. Forcing at $C_\mu = 2.1\%$, as mentioned above, was incapable of fully controlling moment stall, but increased $C_{m,\min}$ by 0.05 and significantly reduced lift hysteresis. A threshold C_μ of approximately 4.6% was required to maintain $C_{m,\text{exe}}$ commensurate with "pre-stall values" ($C_{m,A}$ was increased to 0.07 to account for the larger α excursions based on total elimination of stall; see fig. 11 below). Moreover, $C_{l,\max}$ was increased by approximately 0.2, which was not observed at lower C_μ. This is because the baseline case bubble burst and shed completely from the airfoil while it was still pitching up, and this process was significantly ameliorated with control. Similar results were observed at $k = 0.1$ (not shown) despite more severe baseline stall (i.e. $C_{m,\text{exe}} = 0.25$).

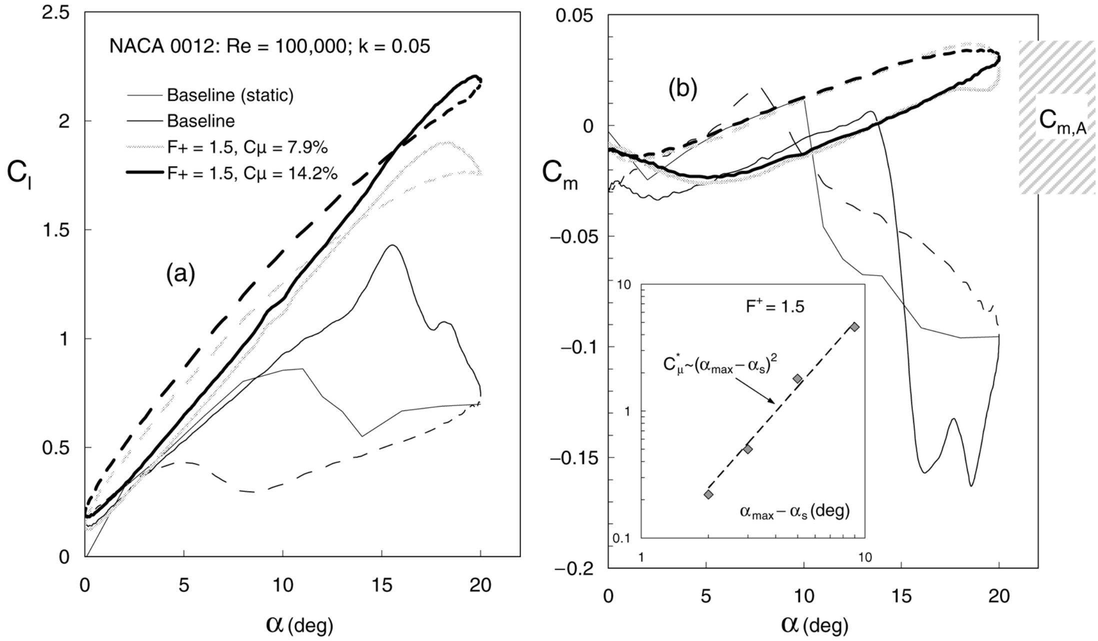

Figure 11. NACA 0012 deep dynamic stall control (45° slot) at relatively high excitation amplitudes: k = 0.05. (Inset: Minimum C_μ required to effect dynamic stall control.)

Note that for a typical slot width $h = 0.01c$, the peak slot velocities are required to be approximately twice the free-stream velocity to obtain C_μ of this magnitude. Thus, compressibility may become a factor when extrapolating these results to conditions at flight Mach numbers ($0.3 \le Ma \le 0.5$). Nevertheless, it should be noted that these C_μ are relatively small in the context of control by means of steady blowing, where typically $16\% \le C_\mu \le 56\%$ are required to produce meaningful changes to the aerodynamic coefficients [22].

Even though significant control is exerted over $C_{m,\text{exe}}$ at $C_\mu = 4.6\%$, light lift and moment stall were evident near $\alpha_{\max}$ for both $k = 0.05$ and $k = 0.1$. Further increases in C_μ resulted in significant additional control authority (figs. 11a and 11b). Indeed, evidence of separation was only fully eliminated for $C_\mu > 10\%$ as can be seen from the C_m vs. α histories which show no negative tendency near $\alpha_{\max}$ at $C_\mu = 14.2\%$ ($C_{m,A}$ was based on $1.2 \times C_{m,\text{exe}}$ at $C_\mu = 14.2\%$). As such, fully attached flow prevails on the upper surface as is evident from $C_{l,\max}$, which is the value predicted in the baseline inviscid limit. In similar fashion to the lower amplitude forcing, the high amplitude forcing essentially traps the vortex at the leading edge as can be seen by the constant pressure region upstream of the slot in figs. 12 and the sharp pressure rise immediately downstream of the slot. Indeed, a large fraction of the overall lift results from the powerful vortical flow upstream of the slot even though this is only 5% of the chord length (figs. 12). Further increases in C_μ also resulted in significant drag reduction and at $C_\mu \approx 8\%$ the mean airfoil drag was eliminated while yet further increases result in thrust generation (see inset in fig. 12).

Deep stall data acquired on the 0015 airfoil (see [9]) indicated that low amplitude forcing ($C_\mu = 0.1\%$) was capable of exerting significant control over moment stall, reducing it by a factor of 2, although $C_{m,\text{exe}} > C_{m,A}$. Moreover, lift hysteresis was significantly attenuated, although $C_{l,\max}$ was not increased. An order

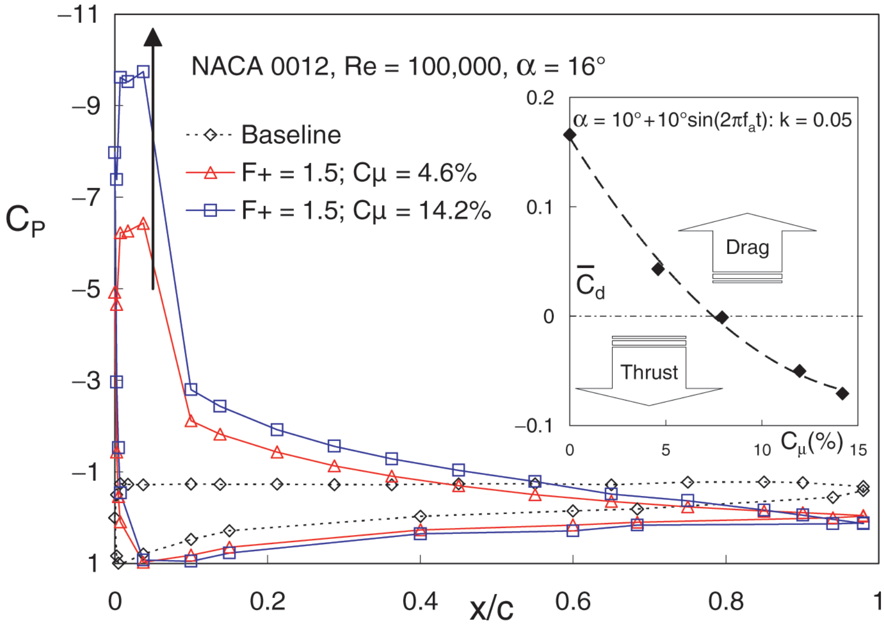

Figure 12. Example of baseline and controlled pressure distributions illustrating the bubble "trapping" near the leading-edge using the 45° slot. (Inset: drag or thrust coefficient as a function of C_μ.)

of magnitude increase in C_μ resulted in virtually no change to $C_{m,\mathrm{exe}}$ although $\Delta C_{l,\max}$ = 38%. High amplitude control (C_μ > 2%, Re < 200,000) data was not acquired on the 0015 airfoil.

Baseline and controlled cases for a further 5º increase in 0012 α_{mean} [i.e. $\alpha = 15^\circ + 10^\circ\sin(2\pi f_a t)$], corresponding to "very deep stall," are presented in figs. 13a and 13b. In this instance, stall is yet deeper as the bubble (or DSV) is shed from the airfoil while it is still pitching-up and moment excursions are excessive ($C_{m,\mathrm{exe}} \approx 0.25$). Forcing at C_μ = 14.2% significantly attenuates the DSV and eliminates moment stall, but it is unable to fully attach the boundary layer for $\alpha > 20°$. In fact, $C_{l,\max}$ was not increased at all when compared with the same forcing amplitude at $\alpha_{\mathrm{mean}} = 10°$ (c.f. figs. 11a) since in the latter case forcing was capable of producing fully attached flow. Therefore, for the present case, dynamic stall is controlled by forcing but no benefit is apparent when compared to the lower α_{mean}.

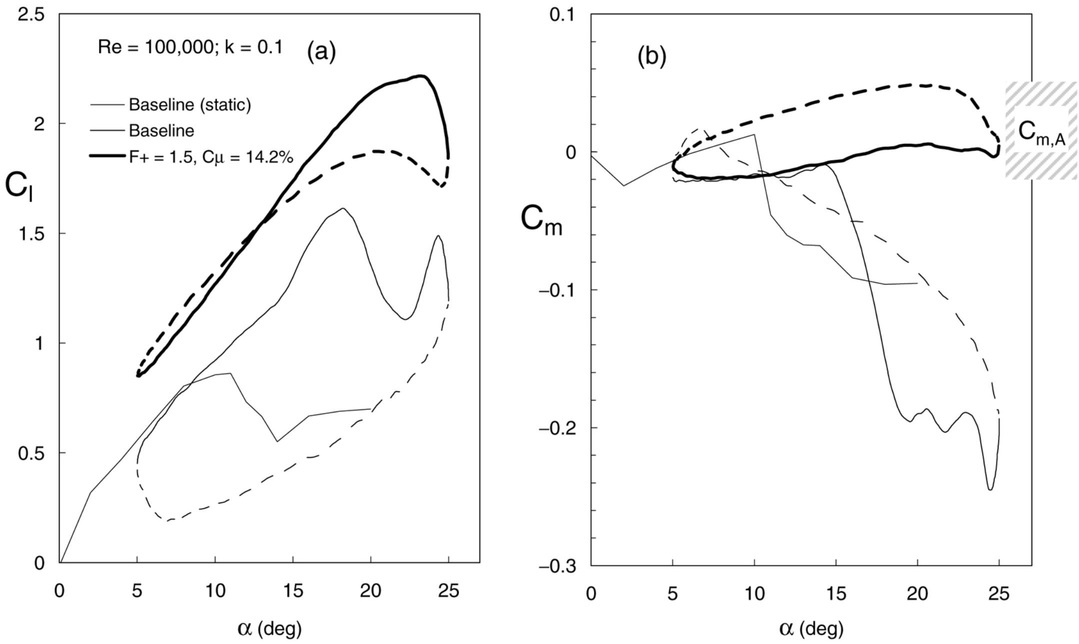

Figure 13. NACA 0012 very deep dynamic stall control (45° slot) at relatively high excitation amplitudes: $k = 0.1$.

Furthermore, $\bar{C}_{dp}$ increased by a factor of 2.4 and thus the drag penalty associated with the present case rendered it inferior. Thus, even when C_m is effectively controlled and C_l is maintained or enhanced, increases in α do not necessarily translate to performance benefits. In such instances, $\bar{C}_d$ or $\bar{C}_{dp}$ should be used as additional indicators of control efficacy. Further considerations, based on the metric described in [13], are discussed below.

3.6. Minimum Momentum Coefficient Required for Control

The inset in fig. 11b shows the minimum momentum coefficient (C_μ^*) required to produce $C_{m,\mathrm{exc}} \le C_{m,A}$ while maintaining or increasing C_l as a function of post-stall angle ($\alpha_{\max} - \alpha_s$) based on data at $F^+ = 1.5$ for Re = 240,000 and 100,000. It is observed that the minimum forcing amplitude required to reduce eliminate dynamic stall can be adequately described by:

$$C_\mu^* = 0.062(\alpha_{\max} - \alpha_s)^2[\%];\ \alpha \text{ in degrees, } 45° \text{ slot} \tag{2}$$

as shown on the figure inset. This relationship may be used to estimate control amplitudes required at higher Reynolds numbers and mild compressibility ($Ma \le 0.35$; see [10]).

The 0012 dynamic stall functions of [13] is shown together with the present baseline data (open symbols) and controlled data (filled symbols) for $0.05 \le k \le 0.015$ (fig. 14a and 14b). Note that only control data that corresponds to $C_{m,\mathrm{exc}} \le C_{m,A}$ (alternatively $C_\mu \ge C_\mu^*$) is plotted. In general, the present baseline data lie below the dynamic stall function data due to the order of magnitude difference in Re between this data and that used to construct the dynamic stall functions. Apart from the very deep stall case ($\alpha_{\max} - \alpha_s = 14°$) the present baseline data can also be fairly well represented by similar functions as those shown in the figures.

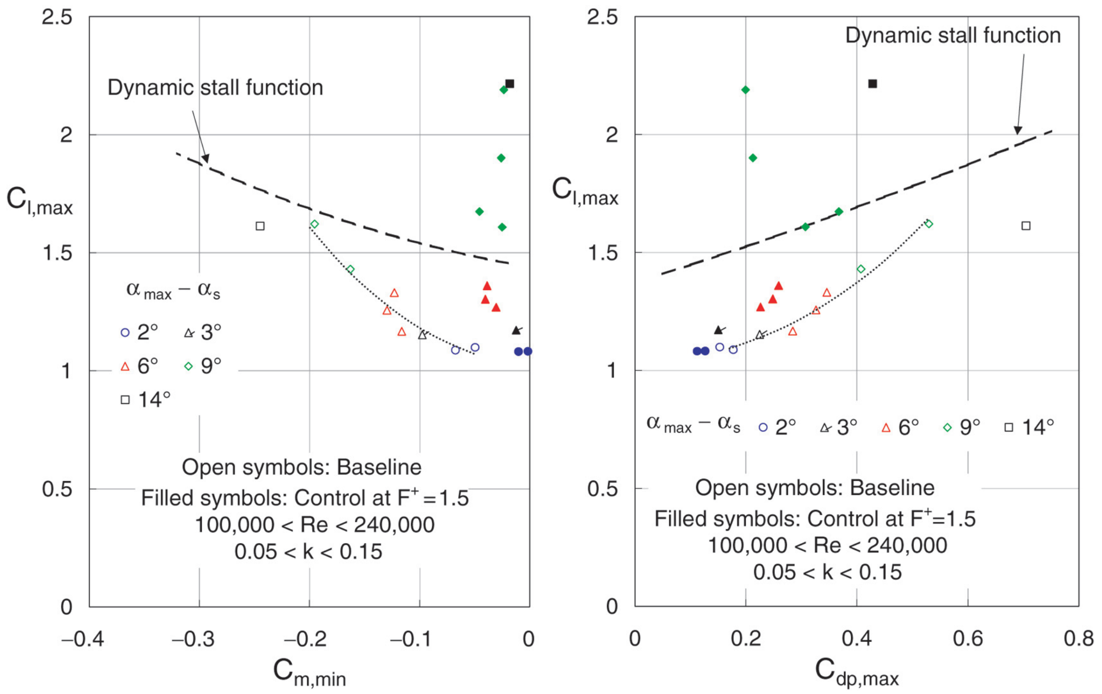

Figure 14. Bouseman's [13] dynamic stall function for the NACA 0012 airfoil, together with baseline and control data.

Clearly, the controlled data sets should be contrasted with the low Reynolds number dynamic stall functions to assess control authority. From fig. 14a it is clear that relatively small changes to $C_{l,\max}$ are accompanied by significant reductions in $C_{m,\min}$. Corresponding changes to $C_{dp,\max}$, on the other hand, depend more strongly on C_μ as can be seen form the data points plotted for the deep stall case ($\alpha_{\max} - \alpha_s = 9°$). As alluded to in the previous section, it is also seen that control at ($\alpha_{\max} - \alpha_s = 9°$) is superior to that at ($\alpha_{\max} - \alpha_s = 14°$) due to the higher $C_{dp,\max}$ associated with the latter.

4. CONCLUDING REMARKS

Control of dynamic stall by means of two-dimensional zero mass-flux oscillatory forcing on a NACA 0012 airfoil yielded the following main conclusions:

1. Dynamic stall could be effectively controlled by "trapping" the bubble upstream of the forcing slot location, in a similar manner to that observed in the static case.
2. Moment coefficient excursion control was most effective with the forcing slot orientated at 45°, as opposed to 90°, to the chord line.
3. The minimum C_μ required to effectively control dynamic stall was observed to be proportional to $(\alpha_{max} - \alpha_s)^2$.
4. Deep dynamic stall was effectively eliminated, but relatively large forcing amplitudes ($C_\mu > 4\%$) were required to effect control.
5. A comparison of NACA 0012 and 0015 airfoils showed that for the former, stall was significantly more severe, typically requiring higher forcing amplitudes (C_μ) for effective control of the moment excursions. Moreover, different F^+ ranges for effective control, consistent with static separation control, were found to be effective for dynamic stall control.

REFERENCES

1. Carr, L.W., "Progress in the analysis and prediction of dynamic stall" *AIAA Journal of Aircraft,* Vol. 25, No. 1, 1988, pp. 6–17.
2. Prouty, R.W., "Helicopter performance, stability and control", PWS Engineering, 1986.
3. Bousman, W.G., "A Qualitative examination of dynamic stall from flight test data", *Journal of the American Helicopter Society,* Vol. 43, October 1998, pp. 279–295.
4. Carr, L.W. and McAlister, K.W., "The effect of a leading-edge slat on the dynamic stall of an oscillating airfoil", AIAA Paper 83–2533, AIAA/AHS Aircraft Design System and Operations Meeting, 1983.
5. Alrefai, M. and Acharya, M., "Controlling leading-edge suction for the management of unsteady separation over pitching airfoils," AIAA Paper 95–2188, *26th AIAA Fluid Dynamics Conference,* June, 1995.
6. P. Lorber, P., McCormick, D., Anderson, T., Wake, B. and MacMartin, D., Pollack, M., Corke, T., Breuer, K., "Rotorcraft retreating blade stall control", AIAA Paper 2000–2475, FLUIDS 2000 Conference and Exhibit, Denver CO, 19–22 June 2000.
7. Geissler, W., Dietz, G., Mai, H., Junker, B., Lorkowski, T., "Dynamic stall control investigations on a full size chord blade section," 30th European Rotorcraft Forum, Marseilles, France, 14–16 September 2004.
8. De Hugues, P.P., McAlister, K.W. and Tung, C., "Effect of an Extendable Slat on the Stall Behavior of a VR-12 Airfoil", NASA TP 3407, September 1993.
9. Greenblatt, D. and Wygnanski, I., "Dynamic stall control by periodic excitation. Part 1: NACA 0015 Parametric Study", *AIAA Journal of Aircraft,* Vol. 38, No. 3, 2001, pp. 430–438.
10. Nagib, H., Greenblatt, D. and Kiedaisch, J., Wygnanski, I and Hassan, A., "Effective flow control for rotorcraft applications at flight Mach numbers", AIAA Paper 2001–2974, 19th AIAA Applied Aerodynamics Conference, Anaheim, California, 11–14 Jun 2001.
11. McCormick, D.C., Lozyniak, S., MacMartin, D.G., and Lorber, P.F., "Compact high power boundary layer separation control actuation development", ASME Fluids Engineering Division Summer Meeting, New Orleans, May 2001. ASME FEDSM2001–18279.
12. Greenblatt, D. and Wygnanski, I., "Effect of leading-edge curvature on airfoil separation control", *AIAA Journal of Aircraft,* Vol. 40, No. 3, 2003, pp. 473–481 (also see AIAA Paper 2002–0411).
13. Bousman, W.G., "Evaluation of airfoil dynamic stall characteristics for maneuverability", 26th European Rotorcraft Forum, The Hague, Netherlands, 26–29 September, 2000, pp. 38.1–38.21.
14. Currier, J.M. and Fung, K.-Y., "Analysis of the onset of dynamic stall", *AIAA Journal,* Vol. 30, pg. 2469, 1992.
15. Van Dommelen L. and Shen, S.F., "The spontaneous generation of the singularity in a separating laminar boundary layer", Journal of Computational Physics, Vol. 38, Nov.–Dec., 1980, pp. 125–140.

16. Pope, A. "The Forces and Moments over an NACA 0015 Airfoil", Aero Digest, Vol. 58, No. 4, 1949, pp. 76,78, and 100.
17. Piziali, R.A., "2-D and 3-D oscillating wing aerodynamics for a range of angles of attack including stall", NASA TM 4632, 1994.
18. Greenblatt, D. and Wygnanski, I, "Control of separation by periodic excitation", Progress in Aerospace Sciences, Volume 37, Issue 7, pp. 487–545, 2000.
19. Saric, W.S., "Görtler Vortices", Annual Review of Fluid Mechanics, Vol. 26, pp. 379–409, 1994.
20. Naim, A., Greenblatt, D., Seifert, A. and Wygnanski, I., "Active Control of a Circular Cylinder Flow at Transitional Reynolds Numbers," Flow, Turbulence & Combustion, Vol. 78, Nos. 3-4, pp.383-407, June, 2007.
21. McCroskey, W.J., "Unsteady Airfoils", Annual Review of Fluid Mechanics, Vol 14, pp 285–311, 1982.
22. Weaver, D., McAlister K.W. and Tso, J., "Control of VR-7 Dynamic Stall by Strong Steady Blowing", *AIAA Journal of Aircraft,* Vol. 41, No. 6, 2004, pp. 1404–1413.
23. Greenblatt, D., Kiedaisch, J. and Nagib H., "Unsteady-pressure corrections in highly attenuated measurements at moderate Mach numbers," AIAA paper 2001–2983, 31st AIAA Fluid Dynamics Conference and Exhibit, Anaheim, CA, June 11–14, 2001.
24. Katz, K. and Plotkin, A., "Low-Speed Aerodynamics," 2ed, Cambridge University Press, 2001, pp.369–447.
25. Greenblatt, D., Nishri, B., Darabi, A. and Wygnanski, I., "Dynamic Stall Control by Periodic Excitation. Part 2: Mechanisms", *AIAA Journal of Aircraft,* Vol. 38, No. 3, 2001, pp. 439–447.
26. McCroskey, W.J., "A Critical Assessment of Wind Tunnel Results for the NACA 0012 Airfoil", Presented at the AGARD FDP Symposium on Aerodynamic Data Accuracy and Quality, Naples, NASA TM 100019, 1987.
27. Piziali, R.A., "2-D and 3-D Oscillating Wing Aerodynamics for a Range of Angles of Attack Including Stall", NASA TM 4632, 1994.
28. Bachar, T., "Generating Dynamically Controllable Oscillatory Fluid Flow", US Patent 6,186,412, Feb. 13,2001.
29. Greenblatt, D., Paschal, K., Yao, C., Harris, J., "A Separation Control CFD Validation Test Case Part 2: Zero Efflux Oscillatory Blowing," AIAA Journal, Vol. 44, No. 12, 2006, pp.2831-2845.
30. McCroskey, W.J., McAlister, K.W., Carr, L.W., Pucci, S.L., and "An Experimental Study of Dynamic Stall on Advanced Airfoil Sections. Volume 2. Pressure and force data" NASA TM 84245, Vols. I-III, 1982.
31. Yu, Y.H., Lee, S., McAlister, K.W., Tung, C., and Wang, C.M., "Dynamic Stall Control for Advanced Rotorcraft Application," *AIAA Journal,* Vol. 33, No. 2, 1995, pp. 289–295.
32. Carr, L.W., Chandrasekhara, M.S., Wilder, M.C., and Noonan, K.W., "Effect of Compressibility on Suppression of Dynamic Stall Using a Slotted Airfoil," Journal of Aircraft, Vol. 38, No. 2, 2001, pp. 296–309; also AIAA Paper 98–0332, Jan. 1998.
33. Chandrasekhara, M.S., Wilder, M.C., and Carr, L.W., "Compressible Dynamic Stall Control Using Dynamic Shape Adaptation," *AIAA Journal,* Vol. 39, No. 10, 2001, pp. 2021–2024; also AIAA Paper 99–0655, Jan. 1999.
34. Chandrasekhara, Martin, P. B. and Tung, C., "Compressible Dynamic Stall Control Using a Variable Droop Leading Edge Airfoil," *AIAA Journal of Aircraft,* Vol. 41, No. 4, 2004, pp. 862–869.
35. Chandrasekhara, M.S., Wilder, M.C., and Carr, L.W., "On the Competing Mechanisms of Compressible Dynamic Stall," *AIAA Journal,* Vol. 36, No. 3, 1998, pp. 387–393; also AIAA Paper 96–1953, June 1996.
36. Neuendorf, R. & Wygnanski I., "On a turbulent wall jet flowing over a circular cylinder", *J. Fluid Mech.,* Vol. 381, pp. 1–25, 1999.
37. Nishri, B. and Wygnanski, I. "Effects of periodic excitation on turbulent separation from a flap", *AIAA Journal,* Vol. 36, No. 4, 1998, pp. 547–556.
38. Darabi, A. and Wygnanski, I., "Active management of naturally separated flow over a solid surface. Part 2. The separation process", *J. Fluid Mech.* Vol. 510, 2004b, pp. 131–144.

39. Park, Y.W., Lee, S. -G., Lee, D. -H. and Hong, S., "Stall Control with Local Surface Buzzing on a NACA 0012 Airfoil", *AIAA Journal,* Vol. 39, No. 7, 2001, pp. 1400–1402.
40. Schmidt, G.S. and Mueller, T.J., "Analysis of Low Reynolds Number Separation Bubbles Using Semi-Empirical Methods", *AIAA Journal,* Vol. 27, No. 8, pp. 993–1001, 1989.
41. Seifert, A., Darabi, A. and Wygnanski, I., "Delay of airfoil stall by periodic excitation", AIAA Journal of Aircraft, Vol. 33, No. 4, 1996, pp. 691–698.